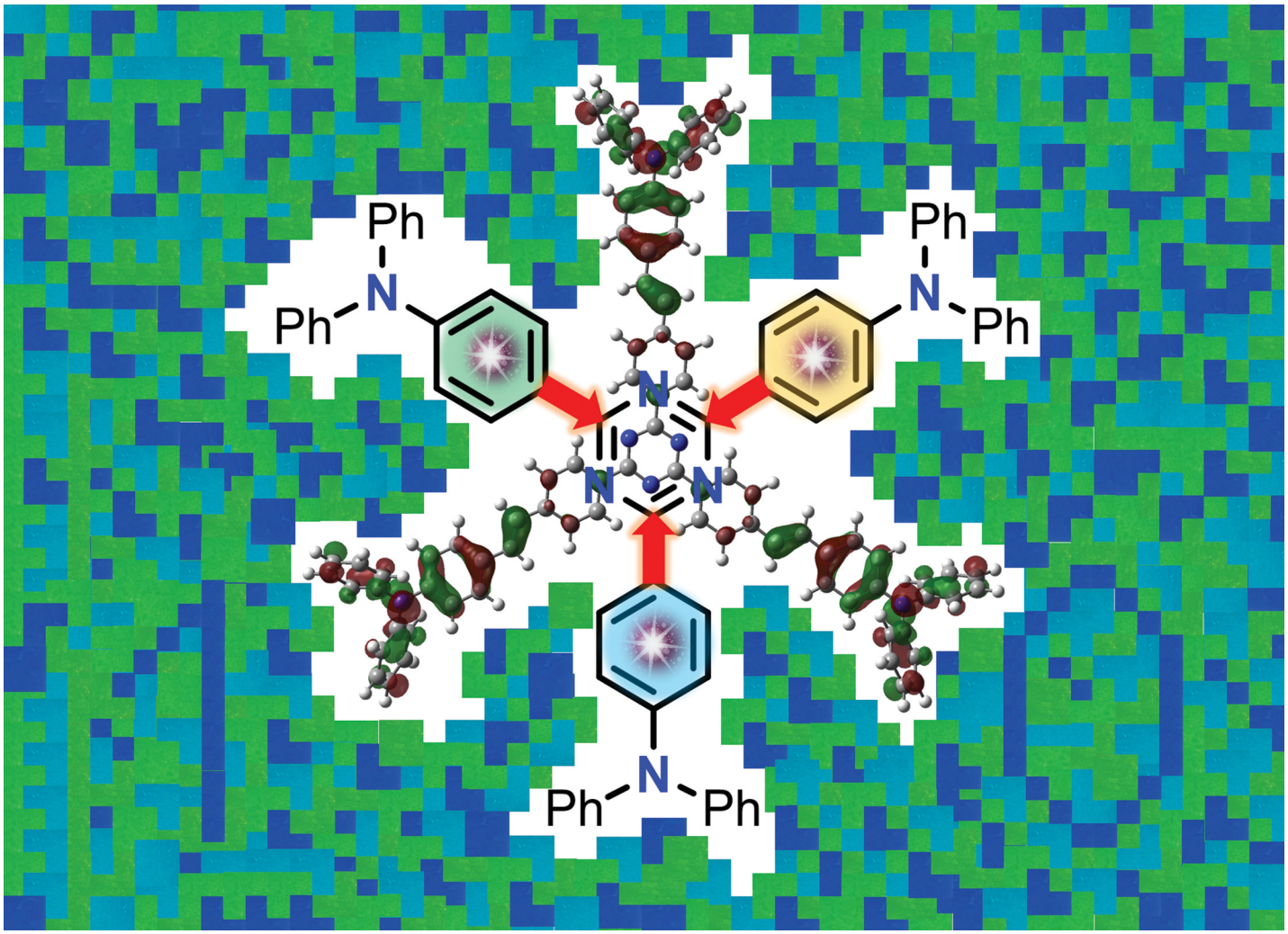

Showcasing a fruitful collaboration of two academic research teams from Czechia and Greece with a commercial company, towards tripodal push–pull chromophores.

Centripetal triazine chromophores: towards efficient two-photon absorbers and highly emissive polyimide films

These extraordinarily arranged centripetal chromophores proved to be efficient two-photon absorbers as well as emitters for fabrication of high-quality polyimide film.

As featured in:

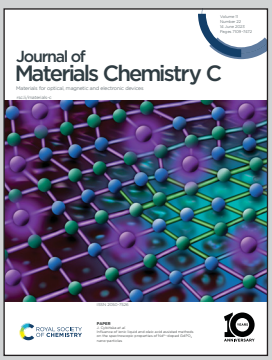

See Mihalis Fakis, Filip Bureš *et al.*, *J. Mater. Chem. C*, 2023, **11**, 7252.

ROYAL SOCIETY OF CHEMISTRY

rsc.li/materials-c

Registered charity number: 207890

Journal of Materials Chemistry C

ROYAL SOCIETY OF CHEMISTRY

PAPER

View Article Online
View Journal | View Issue

Cite this: J. Mater. Chem. C, 2023, 11, 7252

Centripetal triazine chromophores: towards efficient two-photon absorbers and highly emissive polyimide films†

Pavel Šimon, [ab] Milan Klikar, [a] Zuzana Burešová, [a] Chrisovalantou Vourdaki,[c] Alexandros Katsidas,[c] Jiří Tydlitát, [a] Jiří Kulhánek, [a] Jiří Zelenka, [b] Mihalis Fakis *[c] and Filip Bureš *[a]

Received 10th March 2023,
Accepted 10th May 2023

DOI: 10.1039/d3tc00877k

rsc.li/materials-c

Four centripetal (D–π–)$_3$–A chromophores based on *s*-triazine central acceptors and three amino donor-terminated branches were prepared. These chromophores were proved to be thermally stable up to 300 °C with a tuneable HOMO–LUMO gap (3.02–2.51 eV) and longest-wavelength absorption/emission maxima within the range of 390–427/485–551 nm. Relatively large Stokes shift up to 8000 cm^{-1}, quantum yields up to 78% and fluorescence lifetimes ranging between 2 and 4 ns were observed based on the chromophore structure and the used environment. In general, varying the π-linker is proved to be a very useful strategy to tune the fundamental properties of these chromophores. Two-photon absorption measurements showed good to excellent cross-sections reaching 1000 GM. High-quality and well-transparent polyimide films doped with chromophores (0.1%) were further prepared, and showed bright emission in blue and yellow/green regions.

Introduction

Due to their peculiar and tuneable properties, conjugated π-systems end-capped with electron releasing (D) and withdrawing (A) moieties represent a very attractive group of organic materials.[1] Besides an ordinary linear D–π–A arrangement, these systems can be arranged in different ways by varying the number and character of D, A and π-parts, while the resulting structure may more or less resemble letters. Based on this alphabet-inspired design, the current portfolio of extraordinary push–pull systems includes Y-, X-, V-, T-, L- and H-shaped molecules.[2] Tripodal or star (Y)-shaped push–pull systems that feature three interconnected branches are of particular interest as efficient two-photon absorbing (2PA) molecules. These molecules may adopt two principal arrangements – centrifugal (A–π–)$_3$–D or centripetal (D–π–)$_3$–A.[3] The vast majority of centrifugal push–pull molecules were based on triphenylamine central donors.[4] On the other hand, (symmetric) centripetal Y-shaped systems with a central electron acceptor are scarce.

Aromatic heterocycles such as electron deficient six-membered (di/tri)azines are well-suited as central electron withdrawing moieties.[5] Especially 1,3,5-triazine (*s*-triazine) can be employed for the construction of centripetal systems as it is the only azine scaffold allowing the construction of symmetrical molecules. Moreover, its synthesis and modification are historically well-explored in the chemistry of triazine dyes. Star-shaped triazine derivatives have been utilized as charge-transfer chromophores[6] and fluorophores,[7] emissive layers of organic light-emitting diodes (OLEDs),[8] light harvesters in dye-sensitized solar cells (DSSCs),[9] liquid crystals,[10] polymeric cathode materials of Li-ion batteries[11] or covalent-organic frameworks (COFs). Second- and third-order nonlinear optical (NLO) properties, especially second-harmonic generation (SHG),[12] 2PA[13] and 2PA-initiated polymerization[14] of a few triazine derivatives were also reported.

Aromatic polyimides (PIs) are polymeric materials with high thermal and mechanical robustness utilized across various high-tech areas such as aerospace and aviation, (opto)electronics (PLEDs, SCs, displays, filters, fibres, and lenses), automotive industry, medicine, coatings, membranes, packing, labelling *etc.*[15] Flexible, optically transparent (colourless) and heat-resistant plastic substrates are key materials for these applications. There is a direct relationship between the electronic properties of aromatic diamines and dianhydrides constituting the PI's

[a] Institute of Organic Chemistry and Technology, Faculty of Chemical Technology, University of Pardubice, Studentská 573, Pardubice, 53210, Czech Republic. E-mail: filip.bures@upce.cz; Web: https://bures.upce.cz; Fax: +420 46 603 7068; Tel: +420 46 603 7099
[b] Toseda s.r.o., U Panasonicu 376, Staré Čivice, Czech Republic
[c] Department of Physics, University of Patras, GR-26504, Patras, Greece

† Electronic supplementary information (ESI) available: Syntheses, NMR, HR-MS, thermal properties, electrochemistry, 1PA and 2PA data, calculations, and films. See DOI: https://doi.org/10.1039/d3tc00877k

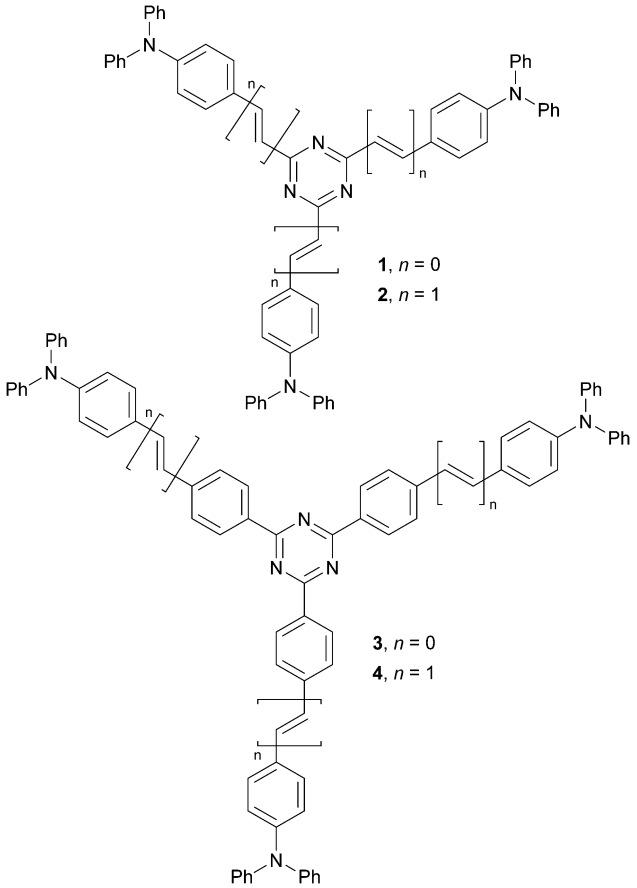

Fig. 1 Molecular structure of centripetal triazine chromophores **1–4**.

structure, while embedding alicyclic and perfluorinated components proved to be a suitable strategy bringing transparency.[16]

Emissive polymeric materials with persisting thermal, chemical and mechanical stability are another important class of organic materials. Due to a variety of additional valuable properties such as (thermally activated delayed) fluorescence, phosphorescence, redox activity and electrochromism, emissive PIs[17] evolved into very attractive and burgeoning macromolecules with manifold applications.[18]

In our previous studies, we focused on star-shaped molecules bearing triphenylamine central donors.[19] Subsequently, we also utilized a variety of azines either as peripheral acceptors or π-linkers.[20] Herein, we report an opposite strategy using *s*-triazine as a central scaffold bearing three peripheral triphenylamines (centripetal $(D–\pi–)_3$–A arrangement). Tripodal chromophores **1–4** (Fig. 1) were synthesized and their fundamental photophysical properties and 2PA activity were examined. These highly emissive fluorophores were further doped into a polyimide made of 1,2,4,5-cyclohexanetetracarboxylic dianhydride and 2,2-bis[4-(4-aminophenoxy)phenyl]propane. In contrast to known emissive PIs, bearing an organic emitter covalently linked to the PI's backbone, our simplified host/guest strategy involves dispersing chromophores **1–4** in the PI matrix.

Results and discussion

Centripetal triazines 1–4

Synthesis. The synthesis of target centripetal chromophores **1–4** is outlined in Scheme 1. In contrast to the published Suzuki–Miyaura reaction of 2,4,6-trichloro-1,3,5-triazine,[21] which proved to be unfeasible as a threefold cross-coupling, 4-(*N*,*N*-diphenylamino)benzaldehyde **5** proved to be a convenient and commercially available starting compound towards

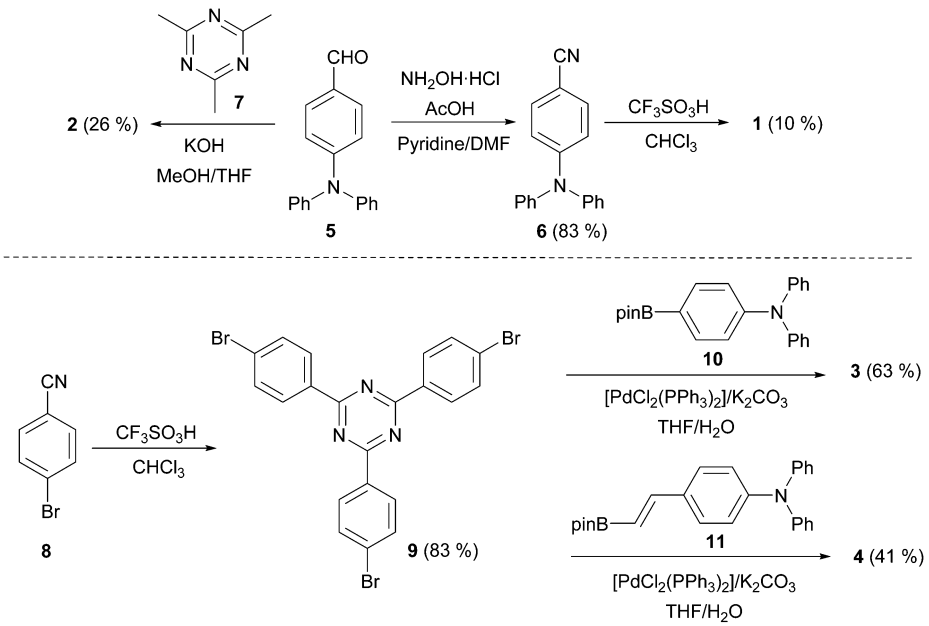

Scheme 1 Synthesis of triazine chromophores **1–4**.

chromophores **1** and **2**. Its treatment with hydroxylamine afforded oxime, which was subsequently transformed into the corresponding benzonitrile **6**.[22] Its acid-catalysed trimerization afforded target chromophore **1** in 10% yield. Despite a relatively low yield, this facile reaction can be performed on a multigram scale. The starting aldehyde **5** also underwent threefold Knoevenagel condensation with 2,4,6-trimethyl-1,3,5-triazine (**7**) to trivinyl chromophore **2** in 26% yield. 2,4,6-Tris(4-bromophenyl)-1,3,5-triazine **9**, prepared by trimerization of 4-bromobenzonitrile **8**,[23] has been utilized in the construction of **3** and **4**. Both chromophores were prepared by threefold Suzuki–Miyaura cross-coupling with pinacol esters **10** and **11** in the yields of 63 and 41%, respectively. Further synthetic details of chromophores **1–4** as well as intermediates are given in the ESI.†

Thermal properties. Thermal characteristics of target chromophores **1–4** were investigated *via* differential scanning calorimetry. The DSC profiles were determined with a scan rate of 10 °C min^{-1} within the range of 25–600 °C. The measured melting points (T_m) as well as the decomposition temperatures (T_d) are summarized in Table 1. All DSC curves are shown in Fig. 2; see the ESI† for individual DSC records. In general, target molecules were isolated as fluffy amorphous powders that underwent a glass transition within the range of 100–110 °C (except **1**). A broad melting process was observed for compounds **1** and **3**, whereas **2** and **4** with embedded olefinic linkers decomposed directly without previous melting. Compounds **3** and **4** bearing additional 1,4-phenylene linkers underwent tedious thermal degradation. Nevertheless, all samples were clearly carbonized after each measurement. The measured T_d values lie within a relatively narrow range of 350–390 °C, which reflects a similar structure of **1–4** based on central triazine and three peripheral *N*,*N*-diphenylamino groups. Hence, compounds **1–4** are considered thermally robust organic chromophores.

Electrochemistry. The electrochemical behaviour of target chromophores **1–4** was investigated *via* cyclic voltammetry (CV) in THF containing 0.1 M Bu_4NPF_6 in a three-electrode cell. The determined peak potentials of the first oxidation and reduction are given *vs.* silver chloride electrode (SSCE). The acquired electrochemical data are summarized in Table 1; further experimental details and recorded CV diagrams are given in the ESI.†

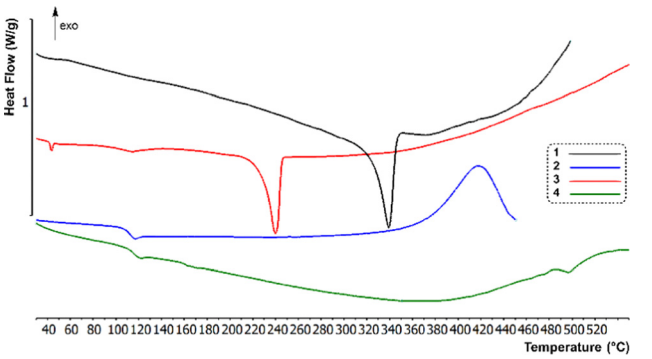

Fig. 2 DSC curves of compounds **1–4** obtained using a heating rate of 10 °C min^{-1} under N_2.

The first reduction of **1–4** was recorded as an electrochemically reversible one-electron process, presumably localized at the central triazine electron-withdrawing unit, followed by subsequent reductions. On the other hand, the first oxidation was determined as an electrochemically irreversible multiple-electron process (peak-to-peak separation around 250 mV) centred on the peripheral *N*,*N*-diphenylamino donors as well as the adjacent π-linker. As deduced from the limit currents $i^a_{p(ox1)}$ and $i^c_{p(red1)}$, four (for **1** and **3**) or seven electrons (for **2** and **4**) were transferred during the first oxidation, which corresponds to the tripodal $(D–\pi)_3$–A character of target chromophores. In addition, a shouldering of the first oxidation peak (see the ESI†), observed for **2** and **4** with embedded double bonds, indicates that the olefinic linker was probably involved in the first oxidation as well. Due to kinetic irreversibility of the first oxidation, the corresponding half-wave potentials are unavailable, therefore peak potentials of the first oxidation and reduction were subtracted to unify the electrochemical data (Table 1). The peak potentials $E_{p(ox1/red1)}$ of **1–4** were found within the range of 1.15 to 1.33 V and −1.36 to −1.69 V, respectively. The $E_{p(ox1/red1)}$ values were further converted to the corresponding HOMO/LUMO energies ($E_{HOMO/LUMO}$), which are depicted in the energy level diagram in Fig. 3, along with the DFT-computed HOMO/LUMO levels. As can be seen, both experimental and calculated data match well and maintain the same trend, especially when considering the shoulder potentials of **2** and **4** (Table 1). When going from **1** to **4**, the

Table 1 A summary of experimental properties of chromophores **1–4**

Comp.	T_m[a] [°C]	T_d[b] [°C]	$E_{p(ox1)}$[c] [V]	$E_{p(red1)}$[c] [V]	ΔE[c] [eV]	E_{HOMO}[e] [eV]	E_{LUMO}[e] [eV]	λ^A_{max}[f] [nm eV^{-1}]	ε[g] [mol^{-1} dm^3 cm^{-1}]	λ^E_{max}[f] [nm eV^{-1}]	Φ^F[h] [%]	Stokes shift [cm^{-1} eV^{-1}]	δ_{2PA}[f] [GM]/ λ^{2PA}_{max} [nm]
1	325	380	1.33	−1.69	3.02	−5.65	−2.63	393/3.16	62 100	485/2.56	74	4830/0.60	205/780
2	—	370	1.20[d]; 1.40	−1.38	2.58	−5.52	−2.94	427/2.90	81 800	525/2.36	52	4370/0.54	620/820
3	229	350	1.25	−1.53	2.78	−5.57	−2.79	390/3.18	70 800	519/2.39	78	6370/0.79	600/770
4	—	390	1.15[d]; 1.32	−1.36	2.51	−5.47	−2.96	418/2.97	107 900	551/2.25	65	5770/0.72	870/830

[a] T_m = melting point (the point of intersection of a baseline and a tangent of thermal effect = onset). [b] T_d = thermal decomposition (pyrolysis under a N_2 atmosphere). [c] $E_{p(ox1)}$ and $E_{p(red1)}$ are peak potentials of the first oxidation and reduction, respectively, as measured by CV at a scan rate of 100 mV s^{-1}; all potentials are given *vs.* SSCE; $\Delta E = E_{p(ox1)} - E_{p(red1)}$. [d] Position of the shoulder of the first oxidation peak. [e] $-E_{HOMO/LUMO} = (E_{p(ox1)} + 0.036)$ and $(E_{p(red1)} + 0.036) + 4.28$ (*vs.* SCE);[24] the increment of +0.036 V corresponds to the difference between the SCE (0.241 *vs.* SHE) and the SSCE (0.205 *vs.* SHE).[25] [f] Measured in THF. [g] Molar absorption coefficient of the longest-wavelength absorption maxima. [h] Fluorescence quantum yield (± 10%) was determined relative to that of 9,10-bis(phenylethynyl)anthracene in cyclohexane (Φ^F = 1.00).[26]

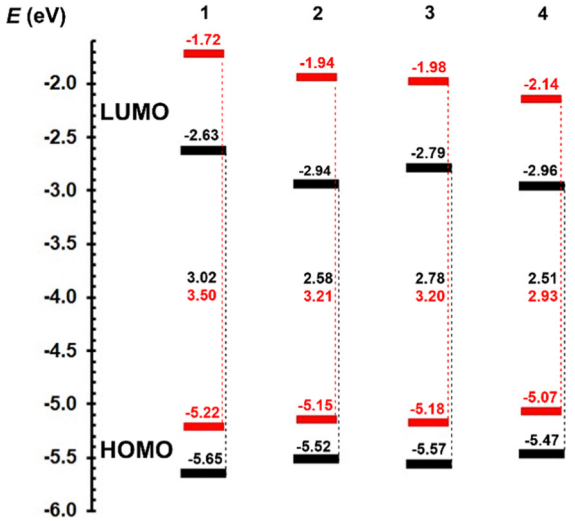

Fig. 3 Energy level diagram of electrochemical (black) and DFT-calculated (red) HOMO and LUMO levels of centripetal triazines **1–4**.

LUMO energy changes more significantly with ΔE_{LUMO} = 0.33 eV as compared to that seen for the HOMO energy (ΔE_{HOMO} = 0.18 eV). Considering the same central triazine acceptor and three peripheral donors, these changes are clearly induced by the π-linker.

The HOMO level increases either with planarization (**1** → **2** or **3** → **4**) or extension (**1** → **3** or **2** → **4**) of the π-linker by olefinic and 1,4-phenylene units. An opposite but more pronounced trends are seen for the LUMO levels. Thus, chromophore **4** with the most extended and planarized stilbenyl π-linker showed the narrowest HOMO–LUMO gap (2.51 eV), which is, however, not large compared to the gap of **2** bearing a styryl π-system (2.58 eV).

One-photon absorption and emission. Fundamental optical properties of chromophores **1–4** were investigated *via* electronic absorption and emission spectra measured in THF, toluene and acetone (Fig. 4 and Fig. S18 in the ESI†). The data acquired for THF are gathered in Table 1; see Table S1 (ESI†) for data of toluene and acetone. The absorption spectra of chromophores **1–4** feature two bands with the peaks appearing at 293–307 and 390–427 nm. While the high-energy bands are mostly attributed to the π–π* transition involving the *s*-triazine core, the low-energy bands at around 400 nm originate from intramolecular charge transfer (ICT). In contrast to known phenoxazine-terminated triazines,[27] the CT bands of **1–4** are very well pronounced and resemble that seen for carbazole-terminated triazines.[28] With the same D and A moieties present in all chromophores, the changes seen in the absorption spectra must be ascribed to the varied π-linker. Its extension by an additional 1,4-phenylene moiety (**1** → **3**) slightly increased the molar absorption coefficient and showed almost no impact on the position of the longest-wavelength absorption maxima. In contrast, an insertion of olefinic subunits (**1** → **2** or **2** → **4**), partially planarizing the π-backbone, resulted in red-shifted CT bands of **2** and **4**. The latter also showed the largest molar absorption coefficient (almost twice as compared to **1**).

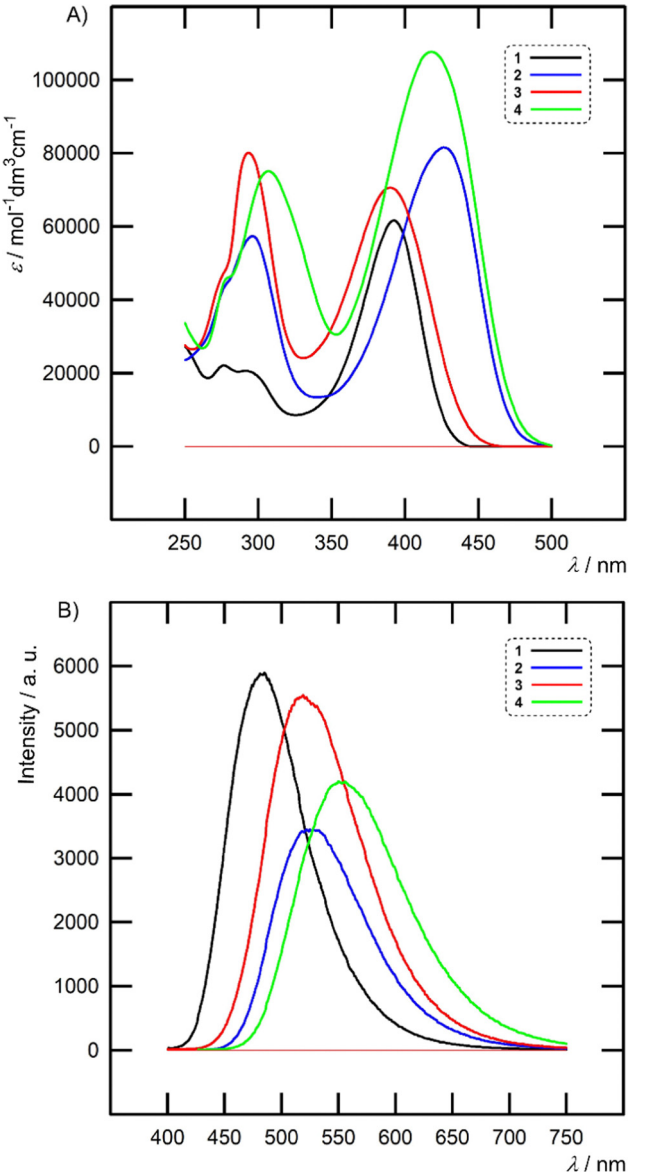

Fig. 4 Absorption (A) and emission (B) spectra of chromophores **1–4** measured in THF ($c = 1 \times 10^{-5}$ mol l^{-1}).

When going from less polar toluene to polar THF, the absorption spectra are affected only negligibly. In contrast, the fluorescence spectra of **1–4** are significantly influenced by the used solvent. For instance, the emission maxima of chromophore **4** are 485 and 551 nm in toluene and THF, respectively.

Hence, the excited state of **1–4** is generally more stabilized by polar solvents, which is also reflected by a larger Stokes shift measured in THF/acetone (4370–6370/6047–8286 cm^{-1}). The highest quantum yields were measured in toluene and Φ^F values decreased steadily when going to THF and acetone. In general, planarized chromophores **2** and **4** with an additional olefinic linker showed lower quantum yields than nonplanar **1** and **3**. Their Φ^F values diminished to almost zero in acetone (Table S1 in the ESI†). Hence, rigid and twisted interconnection of two (hetero)aryls as presented in **1** and **3** allows more

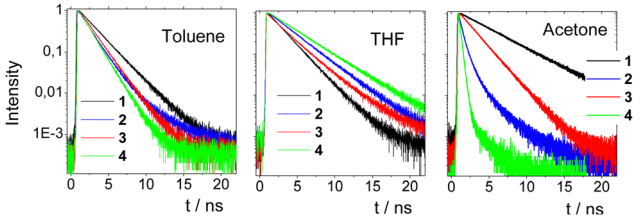

Fig. 5 Fluorescence dynamics of chromophores **1–4** on the ns timescale in three solvents.

efficient and persisted fluorescence as compared to planarized styryl or stilbenyl π-linkers of **2** and **4**. Moreover, concomitant *E*/*Z* photoisomerization may further reduce the quantum yield of **2** and **4**.

Fig. 5 shows the fluorescence decays of chromophores **1–4** in the three solvents while the fitting parameters are summarized in Table S2 (ESI†). The nonplanar molecules **1** and **3** showed simpler decay curves than **2** and **4**, which can be fitted adequately by a single exponential function in almost all cases. In toluene, molecules **1** and **3** exhibit single-exponential dynamics with lifetimes of 2.19 and 1.66 ns, respectively. The lifetime increase in THF becomes 3.78 and 3.08 ns, respectively. This elongation of the lifetime is an indication for an emitting state with different nature. In THF, a more relaxed emitting state with an ICT character is responsible for the emission. In acetone, the dynamics become bi-exponential with a fast component of ∼0.2 ns, indicating non-radiative mechanisms and a longer one due to the emission of the relaxed ICT state.

On the other hand, **2** and **4** show bi-exponential dynamics in all solvents while their dynamics are generally shorter as compared to **1** and **3**. In toluene and THF, the first component (0.5–1 ns) has a smaller amplitude and points to a structural relaxation or to emission from an unrelaxed state, while the second component represents the lifetime of the emitting state (1.5–2.9 ns).[29a,b] The longer component increases from toluene to THF as in the case of **1** and **3** due to the emission from a more relaxed emitting state. In acetone, both molecules exhibit faster dynamics pointing to pronounced non-radiative mechanisms, which is typical in polar solvents.[29a,b]

In order to shed more light on the fast relaxation phenomena of the excited state as well as on solute–solvent interactions, the fluorescence dynamics have also been examined within the first few tens of ps. Fig. 6 shows the dynamics for all molecules in THF, while the results for toluene are given in Fig. S19 (ESI†). All samples in both solvents exhibited fast decays at short wavelengths accompanied by a slow rise at long ones. This behaviour is associated with a gradual relaxation of the excited state and a red-shift of the emission spectrum. The ps dynamics have been fitted using a global method and the results are given in Table S3 (ESI†). In all cases, two relaxation components have were found, while a third component was also found, which corresponds to the lifetime of the excited state (taken from the TCSPC results) and was fixed. Comparing the non-planar and planarized molecules in toluene, the latter exhibit faster dynamics associated to a more efficient ICT

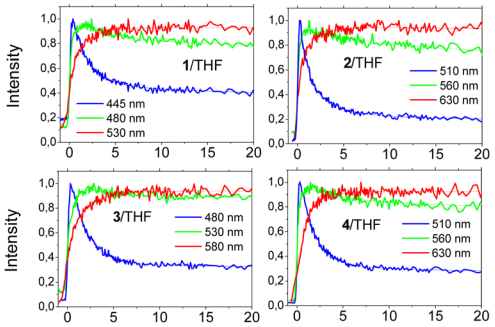

Fig. 6 Fluorescence dynamics of chromophores **1–4** on the ps timescale in THF at different emission wavelengths.

process. For example, compound **2** exhibits relaxation components equal to 0.92 and 5.41 ps *vs.* 1.86 and 7.69 ps found for compound **1**. Besides, in THF, being a more polar solvent, the dynamics are faster than in toluene, which is due to more enhanced solute–solvent interactions meaning that the solutes are facing a stronger solvent reaction field. In THF, a fast relaxation component of ∼1 ps was found for all molecules, which is similar to the average solvation time.[30] The second component can be associated with slower solvation mechanisms as well as ICT formation.

Two-photon absorption properties. Fig. 7 presents the 2PA spectra of compounds **1–4** *i.e.* the 2PA cross-section values, δ_{2PA} *vs.* excitation wavelength in toluene, THF and acetone.

In general, good to excellent 2PA properties have been found with δ_{2PA} reaching 1000 GM. Table 1 summarizes the peak δ_{2PA} for all molecules in THF. More specifically, in all used solvents, the planarized compounds **2** and **4** exhibit larger δ_{2PA} values as compared to those of the non-planarized chromophores **1** and **3**. In THF for example, the larger δ_{2PA} for **4** was found 870 GM (830 nm), while for **3** it was 600 GM (770 nm). Comparing the compounds with or without an additional 1,4-phenylene

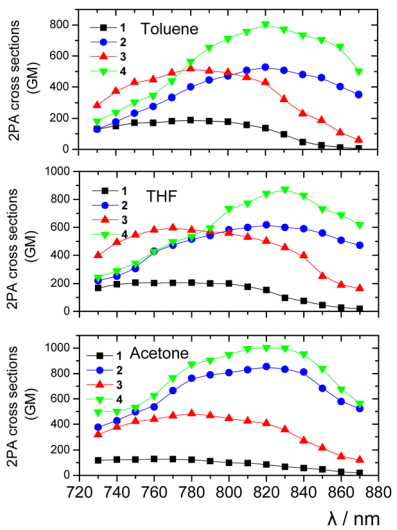

Fig. 7 2PA cross-sections of compounds **1–4** *vs.* wavelengths in the three solvents.

moiety, the former exhibit larger δ_{2PA} values in both planarized and non-planarized series. Overall, the elongation of the conjugated bridge by adding the phenylene moiety and olefinic linkers causes a significant increase in the 2PA activity, rendering compound **4** the most efficient 2PA molecule. Its largest δ_{2PA} was found in acetone (1004 GM at 820 nm). Besides, adding the olefinic subunit also resulted in a red-shift of the 2PA spectra as was the case for the one-photon absorption. Very interesting conclusions can be drawn after comparing the 2PA and one-photon absorption spectra by rescaling them for a better comparison (Fig. S20, ESI†). The 2PA spectra of the non-planarized compounds **1** and **3** almost perfectly match the corresponding one-photon spectra. Such a behaviour is typical for dipolar linear compounds. On the other hand, in tripodal compounds, the excited state splits into three new states, where the two lower-energy states are degenerate. In such case, the lower states can be reached by both 1- and 2-photon transitions, while for the third state, which is higher in energy, only 2-photon transition is allowed.[31] In the case of our tripodal compounds, the resemblance of the one-photon and 2PA spectra can be explained by a small excitonic coupling between the branches. A similar behaviour has been reported for tripodal molecules with a central benzene ring.[32a] For compounds **2** and **4**, however, the 2PA peak is obviously blue-shifted as compared to twice the peak wavelength of the one-photon spectrum (vertical lines are shown in Fig. S20 (ESI†) for a better comparison of the spectral shifts). This means that the higher-lying excited state has the dominant contribution to 2PA, as expected for tripodal compounds with a significant excitonic coupling among the branches. Tripodal molecules having N or C^+ atoms as the central electron donating or accepting core have also exhibited an enhancement of the 2PA efficiency of the higher energy state due to excitonic coupling.[31,32b,c]

As a further step, we tried to correlate the 2PA cross sections with the difference in permanent electric dipole moments between the ground state and the excited state, through the equation[33]

$$\Delta\mu_{2PA} = \left(\frac{5}{4(1+2\cos^2\theta)}\frac{hcN_A}{\pi 10^3 \ln 10 {f_{opt}}^2}\frac{n}{\varepsilon_{max}}\frac{\nu_{max}}{\delta_{2PA}(0-0)}\right)^{1/2} \quad (1)$$

where $\Delta\mu$ is the difference of permanent electric dipole moments between the ground state and the excited state, $\delta_{2PA}(0\text{–}0)$ is the lowest energy peak 2PA cross section, θ is the angle between the dipole moments of the ground and excited state, n is the refractive index (1.41 for THF), f_{opt} is the local field factor equal to $(2 + n^2)/3$, ν_{max} is the lowest energy absorption frequency and ε_{max} is the peak molar absorption coefficient. In performing the calculations, we assumed $\theta = 0$.[33] The values calculated through eqn (1) are summarized in Table S4 (ESI†) and range from 11.8 D for **1** to 19 D for **3**.

Next, these results are compared with those found using the solvatochromism method. In particular, $\Delta\mu$ is related to the slope of the Lippert–Mataga plot through the equation[33c]

$$\Delta\mu_S = \left(hca^3\frac{\Delta\nu}{\Delta F}\right)^{1/2} \quad (2)$$

Table 2 DFT-calculated properties of chromophores **1–4**

Comp.	Symmetry group	E_{HOMO} [eV]	E_{LUMO} [eV]	ΔE [eV]	μ [D]	Cavity radius (Å)
1	D3	−5.22	−1.72	3.50	0	6.23
2	C3	−5.15	−1.94	3.21	0.005	6.41
3	D3	−5.18	−1.98	3.20	0	6.58
4	C3	−5.07	−2.14	2.93	0.011	6.64

where α is the molecular radius assuming that the molecule possesses a spherical cavity (this value has been DFT-calculated, see Table 2) and $\frac{\Delta\nu}{\Delta F}$ is the slope of the Stokes shift in cm^{-1} *versus* the polarity function of the solvent

$$F(\varepsilon, n) = \frac{2(\varepsilon+1)}{2\varepsilon+1} - \frac{2(n^2+1)}{2n^2+1} \quad (3)$$

The $\Delta\mu_S$ values range from 19.1 D to 24.6 D (Table S4, ESI†), showing a noticeable difference from the $\Delta\mu_{2PA}$ value for **1** while being in relatively good agreement with the $\Delta\mu_{2PA}$ values for **2–4**. In general, the $\Delta\mu$ values found are within the same order of magnitude as those found in the literature and point to a significant increase in the polarity of the molecule in the excited state.[33]

Quantum chemical calculations. Fundamental spatial and electronic properties of chromophores **1–4** were analysed with the aid of DFT calculations implemented in the Gaussian W09 package.[34] The optimized geometries of **1–4** were gained using DFT B3LYP/6-31G(d) and B3LYP 6-311G(2d,p) methods. The energies of the frontier molecular orbitals (HOMO and LUMO) and ground state dipole moments (μ) were calculated at the DFT B3LYP/6-311G(2d,p) level and are listed in Table 2. The calculated HOMO/LUMO levels are slightly overestimated as compared to the electrochemical values (see the energy level diagram in Fig. 3) but showed relatively tight correlation (see the ESI†) and the used DFT method is considered a reliable tool for describing electronic properties in the series **1–4**.

Visualization of the frontier molecular orbitals of representative chromophore **4** (Fig. 8, see the ESI† for a full list) reveals the *s*-triazine-centred LUMO including one branch, the LUMO+1 spread over two branches and the LUMO+2 symmetrically localized on the whole π-system. The HOMO is localized on peripheral *N*,*N*-diphenylamino donor moieties, whereas the HOMO−1 and HOMO−2 are spread only over two opposite branches. Hence, a significant charge-transfer is revealed that is further pronounced by extension of the π-system. As expected, the calculated ground state dipole moments are zero for chromophores with D_3-symmetry (**1** and **3**) or close to zero for C_3-symmetrical molecules **2** and **4**.

Polyimide films

Synthesis. Polyimide CHDA–BAPP made of 1,2,4,5-cyclohexanetetracarboxylic dianhydride (CHDA) and 2,2-bis[4-(4-aminophenoxy)phenyl]propane (BAPP) has been selected to prepare emissive films. Its π-conjugated backbone is interrupted by the $(CH_3)_2C$ moiety and cyclohexane ring of BAPP

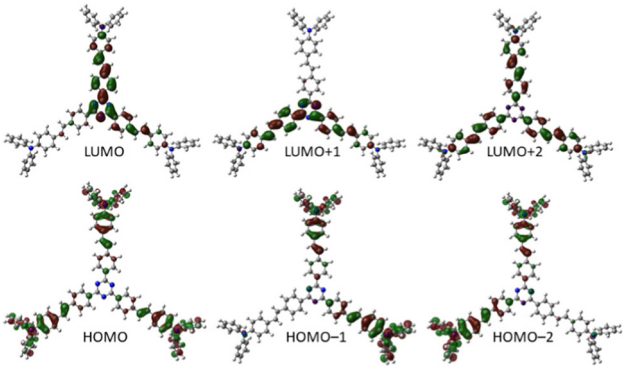

Fig. 8 DFT-calculated visualization of frontier molecular orbitals in representative chromophore **4**.

and CHDA, which significantly reduces its $\lambda_{cut\text{-}off}$ to 295 nm and assures high light-transparency. Persisting mechanical properties along with no crystallization and embrittling upon chromophore doping are other important features of the chosen PI, and are probably given by the elongated structure of the used BAPP amine. CHDA–BAPP was prepared using a conventional two-step thermal imidization method as outlined in Scheme 2, see the ESI† for details. Chromophores **1–4** were embedded into the polymer already during the formation of polyamic acid (PAA), which assured their proper and homogenous distribution. Based on a short concentration study, the chromophore content was optimized to 0.1%, and the thickness of the films was 50 μm.

Thermal stability. Fundamental thermal properties of the prepared polyimide films were investigated by DSC and TGA, as shown in Table 3 and the ESI.† Considering the temperature at which 5% weight loss ($T_d^{5\%}$) occurred, the prepared polyimide CHDA–BAPP proved to be thermally highly stable up to 450 °C. Compared to the structurally related and commercially available Kapton ($T_d^{5\%}$ = 556 °C), CHDA–BAPP is capable of withstanding less heat stress, which is attributed to the aliphatic core of CHDA (cyclohexene *vs.* benzene) and an additional $(CH_3)_2C$ moiety present in BAPP. As judged by the thermal data presented in Table 3, the introduction of triazine chromophores **1–4** (0.1%) into CHDA–BAPP altered its thermal properties negligibly and both glass-transition temperature (T_g) and $T_d^{5\%}$ remained almost unaltered (because of the polyimide backbone).

Optical properties. Optical properties of PI films were evaluated by electronic absorption, transmittance and emission spectra (Fig. 9 and the ESI†); fundamental parameters are listed in Table 3. According to the transmittance shown in Fig. 9(A), the optical window of CHDA–BAPP is significantly broader by almost 200 nm as compared to Kapton ($\lambda_{cut\text{-}off}$ 295 *vs.* 470 nm). This optical feature of CHDA–BAPP, resulting from its partially aliphatic structure, allows its usage as a polymeric matrix for fluorophores emitting in the near UV and Vis region. In contrast to the yellow-orange Kapton, pure CHDA–BAPP is almost fully transparent with no concomitant yellowing (Fig. 9(B)). The reduced T_{400} values of the CHDA–BAPP films doped with **1–4** clearly reflect the presence of the chromophores and their absorption. The colour of the doped films ranges from yellowish to yellow (Fig. 9(B)). Similar to the aforementioned absorptions in solution, triazines **1–4** embedded in CHDA–BAPP showed one longest-wavelength absorption band appearing at 390–430 nm and the high-energy bands (<320 nm) overlapping with the absorption of the PI backbone (Fig. S30, ESI†). The absorption maxima are almost identical to that measured in THF and obey the same trends as seen in solution.

While the pure polyimides (both CHDA–BAPP and Kapton) are non-emissive, the emission spectra of CHDA–BAPP films show one broad band at 461–526 nm depending on the embedded chromophores **1–4** (Fig. 9(D)). The emission maxima are red/blue-shifted ($\Delta\lambda_{max}^{E} \sim$ 10–40 nm) as compared to that measured in toluene/THF (E_T^N = 0.099/0.207).[36] Hence, the polarity of the CHDA–BAPP polyimide can be roughly estimated to lie between those of two solvents. Also, the average fluorescence lifetimes of **1–4** embedded in CHDA–BAPP films were found to lie between the values observed in toluene and THF (Table S5 and Fig. S38, ESI†) except for **2**, whose lifetime in PI is increased and found to be much longer than that in THF.

The film doped with **2** showed significantly enhanced intensity as compared to other chromophores as well as to a CHDA–BAPP film doped with benchmark diphenylanthracene (DPA). While nonplanar chromophores **1** and **3** can be considered as blue emitters (Fig. 9(C)), planarization of the π-backbone by additional olefinic units red-shifted the emission of **2** and **4** to yellow/green colour. Hence, gradual extension and planarization of the chromophore structure allow tuning the emission colour of the films across the CIE chromaticity diagram (Fig. S32, ESI†). Especially CHDA–BAPP + **1** with CIE coordinates

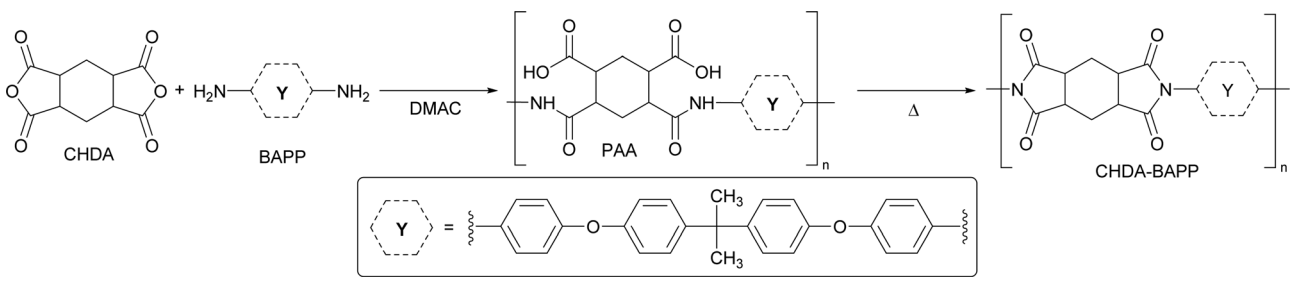

Scheme 2 Molecular structure and preparation of polyimide CHDA–BAPP.

Table 3 Thermal and optical properties of PI films

PI film	$T_d^{5\%}$ [a] [°C]	T_g [b] [°C]	Char yield [c] [wt%]	$\lambda_{cut\text{-}off}$ [nm eV^{-1}]	T_{400} [d] [%]	T_{700} [d] [%]	λ_{max}^{A} [e] [nm eV^{-1}]	λ_{max}^{E} [f] [nm eV^{-1}]	Stokes shift [cm^{-1} eV^{-1}]	Chromaticity CIE [g] (x,y)	FWHM [h] [nm]	$\langle\tau\rangle$ [i] [ns]
CHDA–BAPP	454	258	30	295	86	91	—	—	—	—	—	—
CHDA–BAPP + **1**	449	261	32	293	46	89	392/3.16	461/2.69	3820/0.47	0.165,0.179	72	2.61
CHDA–BAPP + **2**	455	263	30	295	18	89	430/2.88	515/2.41	3840/0.48	0.288,0.531	95	3.44
CHDA–BAPP + **3**	460	262	40	296	53	90	390/3.18	495/2.51	5439/0.67	0.220,0.394	82	2.32
CHDA–BAPP + **4**	455	260	37	294	55	90	416/2.98	526/2.36	5027/0.62	0.333,0566	84	2.09

[a] The temperature at which 5% weight loss occurred was measured by TGA. [b] T_g = glass-transition temperature measured by DSC. [c] Residual weight percentage at 600 °C under the N_2 atmosphere as measured by TGA. [d] Transmittance at 400 and 700 nm, respectively. [e] The longest-wavelength absorption maxima. [f] Emission maxima. [g] CIE coordinates of the emission spectra calculated according to ref. 35. [h] Full-width at half-maximum of the emission spectra. [i] Average lifetimes of **1–4** in PI films.

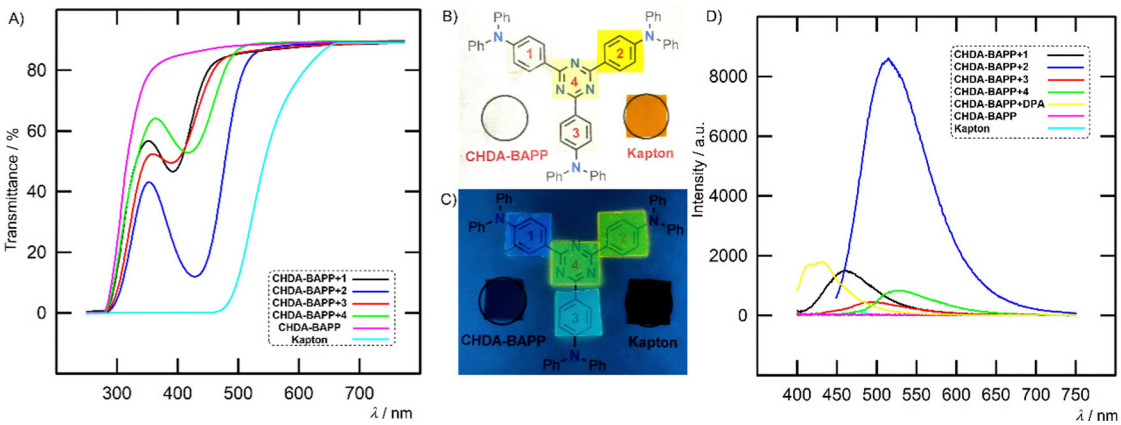

Fig. 9 Transmittance of PI films (A), colour of CHDA–BAPP and films doped with **1–4** (numbered in red) under daylight (B) and 254 nm irradiation (C) and emission spectra of films (D). The spectra and native films (CHDA–BAPP doped with 0.1% of **1–4**) are shown along with the reference Kapton film.

of (0.165, 0.179) can be considered as a promising blue emitter with a relatively narrow emission (FWHM = 72 nm).[37]

Conclusions

A series of star-shaped centripetal push–pull chromophores based on the *s*-triazine central acceptor, three *N*,*N*-diphenylamino donors and a π-linker of systematically varied length have been synthesized and further investigated. These chromophores exhibited thermal stability exceeding 300 °C, while reversible reduction of the triazine core and kinetically irreversible oxidation of the peripheral amino donors were revealed by electrochemistry. A clear trend in tuning the HOMO–LUMO gap *via* extension of the π-system and its planarization *via* an additional olefinic subunit was observed both experimentally and theoretically. Fundamental one- and two-photon absorption and emission properties were screened in various solvents and a distinct intramolecular charge-transfer band was recorded. The emission spectra of chromophores showed one well-resolved band, whose position is strongly influenced by the chromophore structure and the used environment. Single- and bi-exponential fluorescence dynamics were revealed for non-planar and planar chromophores. Planarity and π-system extension also affect two-photon absorption properties, the latter showed significantly enhanced 2PA activity reaching 1000 GM. The synthesized chromophores were further embedded into polyimide films prepared from 1,2,4,5-cyclohexanetetracarboxylic dianhydride and 2,2-bis[4-(4-aminophenoxy)phenyl]-propane. In contrast to benchmark Kapton, these polyimide films are optically well-transparent with thermal robustness persisting up to 450 °C, and can be used as a polymeric matrix for chromophores emitting in the near UV and visible regions. Although the films of nonplanar chromophores emitted in the blue region, planarization and π-linker extension shifted the emission to the yellow/green region. In summary, the developed triazine-derived tripodal chromophores **1–4** proved to be versatile organic materials exhibiting excellent 2PA activity and can be used to prepare emissive polyimide films of high quality.

Experimental section

The detailed syntheses and characterizations of target chromophores **1–4**, intermediates and polyimide films are given in the ESI.†

Author contributions

F. B.: conceptualization. P. Š., M. K., Z. B., C. V., A. K.: investigation. J. T.: software. J. K., J. Z.: supervision. F. B.,

M. F., P. Š., M. K., Z. B.: writing – original draft. F. B., M. F.: writing – review & editing.

Conflicts of interest

There are no conflicts to declare.

Acknowledgements

P. Š. and J. Z. acknowledge the financial support from the Ministry of Education, Youth and Sport of the Czech Republic (CZ.02.1.01/0.0/0.0/17_048/0007376, NANOMAT).

Notes and references

1 F. Bureš, *RSC Adv.*, 2014, **4**, 58826.
2 M. Klikar, P. Solanke, J. Tydlitát and F. Bureš, *Chem. Rec.*, 2016, **16**, 1886.
3 D. Cvejn, E. Michail, I. Polyzos, N. Almonasy, O. Pytela, M. Klikar, T. Mikysek, V. Giannetas, M. Fakis and F. Bureš, *J. Mater. Chem. C*, 2015, **3**, 7345.
4 (*a*) X. Lian, Z. Zhao and D. Cheng, *Mol. Cryst. Liq. Cryst.*, 2017, **648**, 223; (*b*) P. Blanchard, C. Malacrida, C. Cabanetos, J. Roncali and S. Ludwigs, *Polym. Int.*, 2019, **68**, 589; (*c*) A. Karak, S. K. Manna and A. K. Mahapatra, *Anal. Methods*, 2022, **14**, 972; (*d*) A. Mahmood, *Sol. Energy*, 2016, **123**, 127; (*e*) P. Agarwala and D. Kabra, *J. Mater. Chem. A*, 2017, **5**, 1348; (*f*) A. Iwan and D. Sek, *Prog. Polym. Sci.*, 2011, **36**, 1277; (*g*) D. Devadiga, M. Selvakumar, P. Shetty, M. S. Santosh, R. S. Chandrabose and S. Karazhanov, *Int. J. Energy Res.*, 2021, **45**, 6584.
5 (*a*) S. Achelle, J. Rodríguez-López, F. Bureš and F. Robin-le Guen, *Chem. Rec.*, 2020, **20**, 440; (*b*) S. Achelle and N. Plé, *Curr. Org. Synth.*, 2012, **9**, 163.
6 (*a*) J. Hu, Y. Li, H. Zhu, S. Qiu, G. He, X. Zhu and A. Xia, *ChemPhysChem*, 2015, **16**, 2357; (*b*) H. Meier, E. Karpuk and H. C. Holst, *Eur. J. Org. Chem.*, 2006, 2609; (*c*) H. Meier, H. C. Holst and A. Oehlhof, *Eur. J. Org. Chem.*, 2003, 4173.
7 V. S. Padalkar, V. S. Patil and N. Sekar, *Chem. Cent. J.*, 2011, **5**, 77.
8 Y. Zhang, Y. Zheng, B. Wang, H. Ran, X. Wang, J.-Y. Hu and Q. Wang, *J. Mater. Chem. C*, 2020, **8**, 4461.
9 (*a*) H. Zhang, X.-F. Zang, Y.-P. Hong and Z.-E. Chen, *Synth. Met.*, 2021, **280**, 116882; (*b*) J. Liu, K. Wang, F. Xu, Z. Tang, W. Zheng, J. Zhang, C. Li, T. Yu and X. You, *Tetrahedron Lett.*, 2011, **52**, 6492.
10 T. Yasuda, T. Shimizu, F. Liu, G. Ungar and T. Kato, *J. Am. Chem. Soc.*, 2011, **133**, 13437.
11 Z. Chen, C. Su, X. Zhu, R. Xu, L. Xu and C. Zhang, *J. Polym. Sci., Part A: Polym. Chem.*, 2018, **56**, 2574.
12 Y. Z. Cui, Q. Fang, H. Lei, G. Xue and W. T. Yu, *Chem. Phys. Lett.*, 2003, **377**, 507.
13 (*a*) Y. Jiang, Y. Wang, B. Wang, J. Yang, N. He, S. Qian and J. Hua, *Chem. – Asian J.*, 2011, **6**, 157; (*b*) L. Zou, Z. Liu, X. Yan, Y. Liu, Y. Fu, J. Liu, Z. Huang, X. Chen and J. Qin, *Eur. J. Org. Chem.*, 2009, 5587; (*c*) Y. Jiang, Y. Wang, J. Hua, J. Tang, B. Li, S. Qian and H. Tian, *Chem. Commun.*, 2010, **46**, 4689; (*d*) S. Zeng, X. Ouyang, H. Zheng, W. Ji and Z. Ge, *Dyes Pigm.*, 2012, **94**, 290; (*e*) L. Wei, J. P. Shi, Z. Q. Zhou, Y. P. Cui, H. W. Hu and G. Y. Lu, *Chin. Chem. Lett.*, 2012, **23**, 867; (*f*) L. Liu, Z. Q. Zhou, J. P. Shi, C. G. Lu, Y. P. Cui and G. Y. Lu, *Chin. Chem. Lett.*, 2011, **22**, 1147.
14 M. Tromayer, P. Gruber, A. Rosspeintner, A. Ajami, W. Husinsky, F. Plasser, L. González, E. Vauthey, A. Ovsiniakov and R. Liska, *Sci. Rep.*, 2018, **8**, 17273.
15 (*a*) M. Hasegawa, *Polymers*, 2017, **9**, 520; (*b*) P. K. Tapaswi and C.-S. Ha, *Macromol. Chem. Phys.*, 2019, **220**, 1800313; (*c*) H.-J. Ni, J.-G. Liu, Z.-H. Wang and S.-Y. Yang, *J. Ind. Eng. Chem.*, 2015, **28**, 16; (*d*) A. S. Hicyilmaz and A. C. Bedeloglu, *SN Appl. Sci.*, 2021, **3**, 363.
16 (*a*) S. Ando, T. Matsuura and S. Sasaki, *Polym. J.*, 1997, **29**, 69; (*b*) T. Matsumoto, D. Mikami, T. Hashimoto, M. Kaise, R. Takahashi and S. Kawabata, *J. Phys.: Conf. Ser.*, 2009, **187**, 012005; (*c*) H. Yeo, M. Goh, B.-C. Ku and N.-H. You, *Polymer*, 2015, **76**, 280; (*d*) M. Yamada, M. Kusama, T. Matsumoto and T. Kurosaki, *J. Org. Chem.*, 1992, **57**, 6075; (*e*) C. Cao, L. Liu, X. Ma, X. Zhang and T. Lv, *Polim.: Cienc. Tecnol.*, 2020, **30**, e2020017.
17 M. Hagesawa and K. Horie, *Prog. Polym. Sci.*, 2001, **26**, 259.
18 (*a*) Y. Long, X. Chen, H. Wu, Z. Zhou, S. S. Babu, M. Wu, J. Zhao, M. P. Aldred, S. Liu, X. Chen, Z. Chi, J. Xu and Y. Zhang, *Angew. Chem., Int. Ed.*, 2021, **60**, 7220; (*b*) Z. Zhou, Y. Zhang, S. Liu, Z. Chi, X. Chen and J. Xu, *J. Mater. Chem. C*, 2016, **4**, 10509; (*c*) K. Kanosue, S. Hirata, M. Vacha, R. Augulis, V. Gulbinas, R. Ishige and S. Ando, *Mater. Chem. Front.*, 2019, **3**, 39; (*d*) H.-J. Yen, J.-H. Wu, W.-C. Wang and G.-S. Liou, *Adv. Opt. Mater.*, 2013, **1**, 668; (*e*) Z. Zhou, Y. Long, X. Chen, T. Yang, J. Zhao, Y. Meng, Z. Chi, S. Liu, X. Chen, M. P. Aldred, J. Xu and Y. Zhang, *ACS Appl. Mater. Interfaces*, 2020, **12**, 34198; (*f*) A. Iqbal, H. M. Siddiqi, M. Zubair, T. Akhter, O. O. Park and A. Saeed, *High Perform. Polym.*, 2020, **32**, 231; (*g*) A. Iqbal, S. H. Lee, O. O. Park, H. M. Siddiqi and T. Akhter, *New J. Chem.*, 2016, **40**, 5285; (*h*) K. Su, N. Sun, X. Tian, S. Guo, Z. Yan, D. Wang, H. Zhou, X. Zhao and C. Chen, *Dyes Pigm.*, 2019, **171**, 107668; (*i*) Y.-W. Liu, L.-S. Tang, L.-J. Qu, S.-W. Liu, Z.-G. Chi, Y. Zhang and J.-R. Xu, *Chin. J. Polym. Sci.*, 2019, **37**, 416; (*j*) T. Xiao, X. Fan, D. Fan and Q. Li, *Polym. Bull.*, 2017, **74**, 4561.
19 (*a*) K. Seintis, I.-K. Kalis, M. Klikar, F. Bureš and M. Fakis, *Phys. Chem. Chem. Phys.*, 2020, **22**, 16681; (*b*) M. Klikar, K. Seintis, I. Polyzos, O. Pytela, T. Mikysek, N. Almonasy, M. Fakis and F. Bureš, *ChemPhotoChem*, 2018, **2**, 465; (*c*) D. Cvejn, E. Michail, K. Seintis, M. Klikar, O. Pytela, T. Mikysek, N. Almonasy, M. Ludwig, V. Giannetas, M. Fakis and F. Bureš, *RSC Adv.*, 2016, **6**, 12819; (*d*) K. Seintis, D. Agathangelou, D. Cvejn, N. Almonasy, F. Bureš, V. Giannetas and M. Fakis, *Phys. Chem. Chem. Phys.*, 2017, **19**, 16485; (*e*) F. Kournoutas, K. Seintis, N. Karakostas, J. Tydlitát, S. Achelle, G. Pistolis, F. Bureš and M. Fakis, *J. Phys. Chem. A*, 2019, **123**, 417.
20 (*a*) F. Bureš, D. Cvejn, K. Melánová, L. Beneš, J. Svoboda, V. Zima, O. Pytela, T. Mikysek, Z. Růžičková, I. V. Kityk,

A. Wojciechowski and N. AlZayed, *J. Mater. Chem. C*, 2016, **4**, 468; (*b*) M. Klikar, D. Georgiou, I. Polyzos, M. Fakis, Z. Růžičková, O. Pytela and F. Bureš, *Dyes Pigm.*, 2022, **201**, 110230; (*c*) M. Fecková, I. K. Kalis, T. Roisnel, P. le Poul, O. Pytela, M. Klikar, F. Robin-le Guen, F. Bureš, M. Fakis and S. Achelle, *Chem. – Eur. J.*, 2021, **27**, 1145; (*d*) M. Fecková, P. le Poul, F. Bureš, F. Robin-le Guen and S. Achelle, *Dyes Pigm.*, 2020, **182**, 108659; (*e*) F. Kournoutas, A. Fihey, J.-P. Malval, A. Spangenberg, M. Fecková, P. le Poul, C. Katan, F. Robin-le Guen, F. Bureš, S. Achelle and M. Fakis, *Phys. Chem. Chem. Phys.*, 2020, **22**, 4165.

21 (*a*) Z. Chen, C. Su, X. Zhu, R. Xu, L. Xu and C. Zhang, *J. Polym. Sci., Part A: Polym. Chem.*, 2018, **56**, 2574; (*b*) Y. Zhang, Y. Zheng, B. Wang, H. Ran, X. Wang, J. Y. Hu and Q. Wang, *J. Mater. Chem. C*, 2020, **8**, 4461.

22 W. Li, Y. Dai, C. Zhang and Z. Chen, 2018, CN109053609A.

23 G. Kim, T. Shiraki and T. Fujigaya, *Bull. Chem. Soc. Jpn.*, 2020, **93**, 414.

24 (*a*) T. J. Carter, R. Mohtadi, T. S. Arthur, F. Mizuno, R. Zhang, S. Shirai and J. W. Kampf, *Angew. Chem., Int. Ed.*, 2014, **53**, 3173; (*b*) A. A. Isse and A. Gennaro, *J. Phys. Chem. B*, 2010, **114**, 7894.

25 D. T. Sawyer, A. Sobkowiak and J. L. Roberts, *Electrochemistry for Chemists*, J. Wiley and Sons Inc., 2nd edn, 1995.

26 D. F. Eaton, *Pure Appl. Chem.*, 1988, **60**, 1107.

27 H. Tanaka, K. Shizu, H. Nakanotani and C. Adachi, *Chem. Mater.*, 2013, **25**, 3766.

28 F. Xu, Z. Wang and Q. Gong, *Opt. Mater.*, 2007, **29**, 723.

29 (*a*) M. Fakis, V. Petropoulos, P. Hrobárik, J. Nociarová, P. Osuský, M. Maiuri and G. Cerullo, *J. Phys. Chem. B*, 2022, **126**, 8532; (*b*) A. Cesaretti, T. Bianconi, M. Coccimiglio, N. Montegiove, Y. Rout, P. L. Gentili, R. Misra and B. Carlotti, *J. Phys. Chem. C*, 2022, **126**, 10429.

30 M. L. Horng, J. A. Gardecki, A. Papazyan and M. Maroncelli, *J. Phys. Chem.*, 1995, **99**, 17311.

31 C. Katan, F. Terenziani, O. Morgin, M. H. V. Werts, L. Porrès, T. Pons, J. Mertz, S. Tretiak and M. Blanchard-Desce, *J. Phys. Chem. A*, 2005, **109**, 3024.

32 (*a*) F. Terenziani, C. Le Droumaguet, C. Katan, O. Mongin and M. Blanchard-Desce, *ChemPhysChem*, 2007, **8**, 723; (*b*) J. C. Collings, S. Y. Poon, C. Le Droumaguet, M. Charlot, C. Katan, L. O. Plsson, A. Beeby, J. A. Mosely, H. Martin Kaiser, D. Kaufmann, W. Y. Wong, M. Blanchard-Desce and T. B. Marder, *Chem. – Eur. J.*, 2009, **15**, 198; (*c*) N. S. Makarov, S. Mukhopadhyay, K. Yesudas, J. L. L. Brédas and J. Perry, *J. Phys. Chem. A*, 2012, **116**, 3781.

33 (*a*) M. G. Vivas, D. L. Silva, J. Malinge, M. Boujtita, R. Zalesny, W. Bartkowiak, H. Angren, S. Canuto, L. De Boni, E. Ishow and C. R. Mendonca, *Sci. Rep.*, 2014, **4**, 4447; (*b*) A. Rebane, M. Drobizhev, N. S. Makarov, E. Beuerman, S. Tillo and T. Hughes, *J. Lumin.*, 2010, **130**, 1619; (*c*) A. Rebane, M. Drobizhev, N. S. Makarov, E. Beuerman, J. E. Haley, D. M. Krein, A. R. Burke, J. L. Flikkema and T. M. Cooper, *J. Phys. Chem. A*, 2011, **115**, 4255; (*d*) L. H. Zucolotto Cocca, A. Gasparotto Pelosi, L. M. G. Abegao, R. de, Q. Garcia, J.-C. Mulatier, D. Pitrat, C. Barsu, C. Andraud, C. R. Mendonça, M. G. Vivas and L. De Boni, *Phys. Chem. Chem. Phys.*, 2023, **25**, 5021; (*e*) A. Rebane, M. Drobizhev, N. S. Makarov, G. Wicks, P. Wnuk, Y. Stepanenko, J. E. Haley, D. M. Krein, J. L. Fore, A. R. Burke, J. E. Slagle, D. G. McLean and T. M. Cooper, *J. Phys. Chem. A*, 2014, **118**, 3749.

34 M. J. Frisch, G. W. Trucks, H. B. Schlegel, G. E. Scuseria, M. A. Robb, J. R. Cheeseman, G. Scalmani, V. Barone, G. A. Petersson, H. Nakatsuji, X. Li, M. Caricato, A. V. Marenich, J. Bloino, B. G. Janesko, R. Gomperts, B. Mennucci, H. P. Hratchian, J. V. Ortiz, A. F. Izmaylov, J. L. Sonnenberg, D. Williams-Young, F. Ding, F. Lipparini, F. Egidi, J. Goings, B. Peng, A. Petrone, T. Henderson, D. Ranasinghe, V. G. Zakrzewski, J. Gao, N. Rega, G. Zheng, W. Liang, M. Hada, M. Ehara, K. Toyota, R. Fukuda, J. Hasegawa, M. Ishida, T. Nakajima, Y. Honda, O. Kitao, H. Nakai, T. Vreven, K. Throssell, J. A. Montgomery, Jr., J. E. Peralta, F. Ogliaro, M. J. Bearpark, J. J. Heyd, E. N. Brothers, K. N. Kudin, V. N. Staroverov, T. A. Keith, R. Kobayashi, J. Normand, K. Raghavachari, A. P. Rendell, J. C. Burant, S. S. Iyengar, J. Tomasi, M. Cossi, J. M. Millam, M. Klene, C. Adamo, R. Cammi, J. W. Ochterski, R. L. Martin, K. Morokuma, O. Farkas, J. B. Foresman and D. J. Fox,*Gaussian 16, Revision C.01*, Gaussian, Inc., Wallingford CT, 2019.

35 E. H. H. Hasabeldaim, CIE chromaticity diagram 1931, 2021, **https://sciapps.sci-sim.com/CIE1931.html**.

36 F. Bureš, O. Pytela and F. Diederich, *J. Phys. Org. Chem.*, 2009, **22**, 155.

37 (*a*) X. Yang, X. Xu and G. Zhou, *J. Mater. Chem. C*, 2015, **3**, 913; (*b*) M. Xie, M. Sun, S. Xue and W. Yang, *Dyes Pigm.*, 2022, **208**, 110799.